Journal of Current Science and Technology, July - September 2025 Vol. 15 No. 3, Article 122

ISSN 2630-0656 (Online)

Cite this article: Aruxvanit, S., Kiatsiriroat, T., Deethayat, T., & Asanakham, A. (2025). Experimental study on slurry ice formation in right circular cylinder and its empirical model. *Journal of Current Science and Technology*, *15*(3), Article 122. https://doi.org/10.59796/jcst.V15N3.2025.122

Journal of Current Science and Technology

Journal homepage: https://jcst.rsu.ac.th

Experimental Study on Slurry Ice Formation in Right Circular Cylinder and Its Empirical Model

Sirachat Aruxvanit[1], Tanongkiat Kiatsiriroat[2,3], Thoranis Deethayat[2,3], and Attakorn Asanakham[2,3,*]

[1]Energy Engineering Program, Faculty of Engineering and Graduate School, Chiang Mai University, Chiang Mai 50200, Thailand
[2]Thermal System Research Laboratory, Department of Mechanical Engineering, Faculty of Engineering, Chiang Mai University, Chiang Mai 50200, Thailand
[3]Research Group for Renewable Energy, Faculty of Engineering, Chiang Mai University, Chiang Mai 50200, Thailand

[*]Corresponding author; E-mail: attakorn.asana@cmu.ac.th

Received 31 March 2025; Revised 26 April 2025; Accepted 27 April 2025; Published online 15 June 2025

Abstract

Slurry ice has the potential to serve as a secondary working fluid for cooling purposes or as a cold storage medium due to its high energy intensity. In the latter application, it can overcome the drawbacks associated with using regular ice, such as ice bridging and insulation, thereby enhancing heat transfer between the exchanger surface and the surrounding medium. However, the solidification process depends on various factors, including the concentration of the freezing point depressant, the freezing point of the working medium, the size and shape of the storage medium, and its thermal properties. This study investigated the formation of slurry ice using water-ethanol and water-propylene glycol mixtures with different concentrations of freezing point depressants. The experiments were conducted in a freezer at temperatures around -15 and -20^{o}C. The findings revealed that higher concentrations of freezing point depressants resulted in a faster growth rate of ice, however when the concentration exceeded 8 wt%, the opposite effect was observed. To better understand the process phenomena, a set of new empirical models was developed using polynomial curve fitting of related parameters in dimensionless forms to predict the amount of slurry ice formed over time. The results from the models showed good agreement with the experimental data across different concentrations of freezing point depressants and container sizes.

Keywords: *slurry ice formation; phase change material; right circular container; experimental model*

1. Introduction

Cold energy storage typically stores coolness in terms of sensible heat such as chilled water (San Khun et al., 2025) or water-ethylene glycol (Sawicka et al., 2020), and latent heat in the form of phase change material (PCM) like paraffin and ice. For latent heat storage, due to its higher energy density, the storage size can be smaller compared to that of sensible heat storage (Chavan et al., 2022). The most common medium is ice-water, as it is readily available. In building air conditioning, chilled water from an ice-on-coil system is commonly used, leading to approximately a one-third reduction in peak electrical demand compared to a regular air conditioner without energy storage (Wang, & Kusumoto, 2001). However, when ice forms on the surface of the heat exchanger, poorer heat transfer between the water and the cooling fluid inside the heat exchanger is obtained. This occurs because the ice creates a barrier to heat transfer on the surface, leading to increased electrical energy consumption by the refrigeration unit (Sandström, 2021). Fang et al., (2021) investigated the parameters involving in the solidification of ice on a coil. The relationships among the frozen layer thickness, the coolant bulk temperature, the tube wall temperature, and the energy extracted from the phase-change medium were considered in terms of the coolant Stanton number, the Biot number, and the solid-phase Stefan number. The results revealed a strong correlation with the Biot number rather than the Stanton and Stefan numbers.

In the case of other PCMs, Nguyen, & Tran (2020) conducted experiments to investigate the solidification and melting rates of glycerin, glycol, paraffin, and sodium polyacrylate, compared with water stored in cylindrical bottles. Glycerin was recommended due to its significant temperature reduction rate during the charging process and its extended melting time during discharging, attributed to its high latent heat. Glycerin also exhibited a low melting temperature and resulted in a low temperature of generated chilled water, which remained stable for a longer duration compared to other storage media. Loem et al., (2023) used a packed bed of RT18HC paraffin for cool storage to reduce air temperature before entering the evaporator of an air conditioner during the daytime and the electrical power input of the air conditioner could be reduced by 13.84-16.13%. Rahdar et al., (2016) used RT3HC, a paraffin with melting point of about 3°C, as a storage medium compared with ice thermal energy storage. Since the operating temperature was above freezing, a higher COP for refrigeration was achieved compared to ice. However, the paraffin had a lower latent heat, ranging from 120 -260 kJ/kg (Yang et al., 2020, Jebasingh, & Arasu, 2020), compared to 334 kJ/kg of ice, which meant that the size of paraffin energy storage was larger than that of ice. Similarly, due to the low thermal conductivity of PCMs like paraffin and ice, poor heat transfer performance during solidification was observed, prompting investigations into designs that increase the heat transfer surface of the storage medium. Hamzeh, & Miansari (2020) modified finned tubular coils to increase the heat exchange capacity of ice-on-evaporator coils. A numerical study showed that increasing fin length and tube number, along with reducing tube diameter, resulted in greater ice formation. Afsharpanah et al., (2022a) designed two rows of serpentine tubes equipped with connecting vertical plates to improve charging performance in a small-scale ice container. The geometric aspects of the serpentine tubes and extended surfaces affected the ice formation were investigated, including the serpentine tube pitch length/container height ratio ($\gamma 1$), the serpentine tube row distance/container width ratio ($\gamma 2$), the serpentine tube diameter/container diagonal length ratio ($\gamma 3$), the plate area/maximum plate area ratio ($\gamma 4$), and the plate thickness/tube diameter ratio ($\gamma 5$). The results showed that higher values $\gamma 1$, $\gamma 2$, $\gamma 4$, and $\gamma 5$, and lower $\gamma 3$ values enhanced the charging rates. Afsharpanah et al., (2022b) also presented various anchor-type fin designs fin for a shell-and-tube ice storage system to reduce operating time during phase change. Hamali, & Almusawa (2022) implemented Y-shaped fins with adding CuO nanoparticles into water to enhance the rate of ice solidification in a container. Similar results were reported Li et al., (2023) for radial fins. The freezing time was reduced by 10-11 % compared to that without nanoparticles.

Enhancement of heat exchange performance of PCM storage media has also been achieved using slurry ice which consists of microscopic ice crystals rather than solid ice with a crystalline molecular structure (Kauffeld et al., 2010). During ice formation, slurry ice avoids the disadvantages of ice bridging and insulation effects. During melting, its large surface area allows for efficient heat exchange compared to conventional ice, enabling it to melt quickly and respond to varying cooling loads while maintaining a steady outlet temperature of the working fluid. Various slurry ice generation methods exist, including scraper type (Rayhan et al., 2020a; Han et al., 2020), supercooled phenomenon (Zhang et al., 2019; Kumano et al., 2010), direct contact heat transfer (Chen et al., 2021, Thongwik et al., 2008), and supercooled water jet (Mouneer et al., 2010). The working fluid used to generate slurry ice must be miscible with water such as ethanol, propylene (PP), ethylene glycol (EG), and saline (Rawat, & Pratihar, 2018; Kumano et al., 2007) and the mixture must have a freezing point lower than that of water. When such mixtures are cooled to the point of solidification, flake or slurry ice not crystalline ice forms on the cooling surface. As a result, improved heat exchange between the liquid surrounding the heat exchanger and the cooling surface can be achieved (Ickes, & Cadwallader, 2017). Rawat, & Pratihar (2018) studied the thermophysical properties, such as density, freezing point, and viscosity, of aqueous solutions containing various freezing point depressants (FPDs), including ethanol (EA), ethylene glycol (EG), propylene glycol (PG), and sodium chloride. They found ethanol to be the most suitable for producing slurry ice, as it promoted uniform ice crystallization. Rayhan et al., (2020b) studied the effect of slurry ice mass fraction on the pressure drop in the cooling system.

Slurry ice has been used in various applications, such as storing sea bass to retain flesh quality, reduce trauma compared to ice cubes, which can exert pressure on the fish and extend shelf life during transportation (Li et al., 2023). Slurry ice could also be used as a secondary working fluid for cooling or as a cold storage medium in refrigeration systems for building air conditioning, due to its high energy intensity (Hao et al., 2021).

The solidification process of slurry ice is a complex phenomenon influenced by various factors, including the concentration of the freezing point depressant, the freezing point of the working medium, size or shape of the storage, and the thermal properties of the solution. To date, no comprehensive model is available to accurately predict the amount of slurry ice over time, which serves the primary motivation for the present study. In this work, the formation of slurry ice was experimentally investigated within a right circular cylindrical vessel placed in a controlled freezer environment, where temperatures were maintained at approximately −15 °C and −20 °C. The study utilized water–ethanol and water–propylene glycol mixtures to compare and investigate the influence of FPD concentration on slurry ice formation. A set of novel empirical models, expressed in dimensionless terms and encompassing relevant parameters, was developed and validated against experimental data. The outcomes of this study enhance the understanding of slurry ice phase transitions in confined geometries and establish a robust framework for predicting the amount of slurry ice formed over time. Additionally, the study identified concentration ranges that facilitate rapid slurry ice formation.

2. Objectives

This study aims to investigate the formation and growth behavior of slurry ice using water–ethanol and water–propylene glycol mixtures with varying concentrations of freezing point depressants. The novelty of this work lies in the development of a set of new empirical models capable of predicting the amount of slurry ice formed over time within a right circular cylindrical vessel.

3. Methodology

3.1 Experimental Setup

Eight vertical right circular cylindrical glass containers were used during the experiment. Each container had a diameter of 5.6 cm and a height of 12 cm and it was filled with 7 cm of water or water mixed with ethanol and propylene glycol. The containers were placed in a freezer, where the temperature was controlled at -15±2°C or -20±2°C, as depicted in Figure 1. To ensure proper insulation, both ends of each container were covered with polyethylene foam. For the water-ethanol and water-propylene glycol solutions, concentrations of 2%, 4%, 6%, 8%, 10%, and 12% by weight were used. The freezer dimensions were 15 cm in width, 17 cm in length, and 27 cm in height. Three thermocouples were placed at different locations inside the freezer to monitor and record internal temperatures, which remained consistent. Another thermocouple was installed in one of the containers to measure the temperature of the working medium over time, as shown in Figure 1a.

The temperature of the medium in one container was continuously monitored as shown in Figure 1b, and this reading was used as a reference for the temperatures in the other containers during the cooling process. The experiment started when the liquid in the container reached 20°C. The freezing chamber reached the set temperature within approximately 90 minutes, and ice formation was observed in all containers. After 120 min, the first container was removed. Subsequently, every 30 min, one container was taken out to examine the development and quantity of ice.

A set of K-type thermocouples (HAUTO S220-T8 RANGE -200 to 1800°C) with an accuracy of ±0.2ºC was used in this study. The ice was separated using a fine-mesh strainer, and the masses of both the ice and the liquid solution were subsequently measured using a weighing machine (CST-CDR 30, resolution 1 g). The strainer was vigorously shaken 2–3 times until residual water was no longer visibly dripping. This process was repeated three times, with the deviation from the average value remaining below 8%.

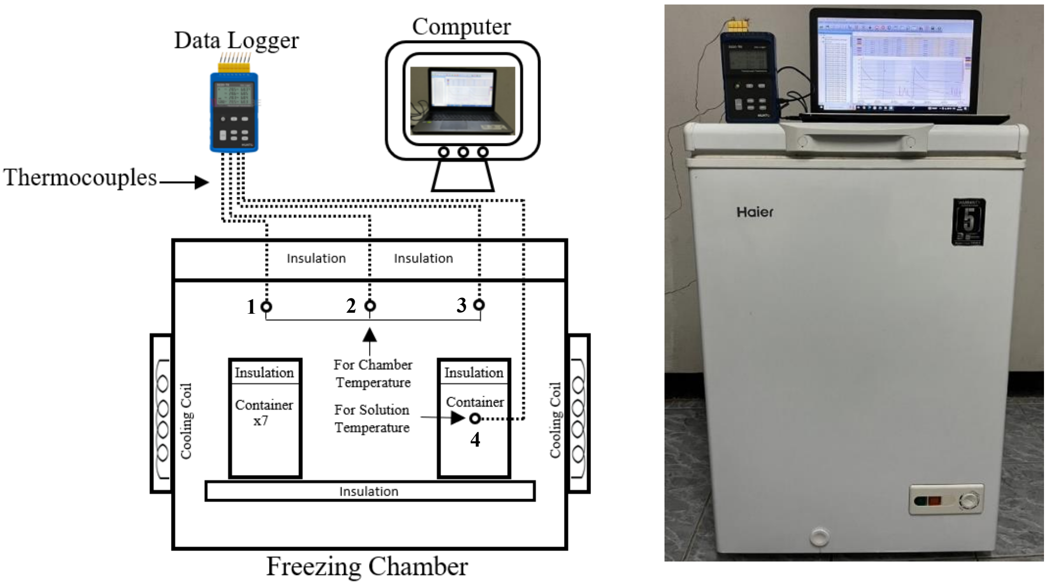

a. Freezing chamber and freezer.

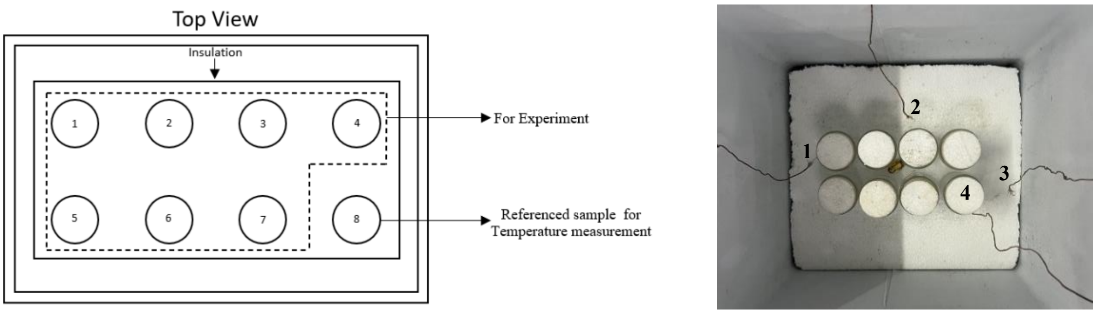

b. Arrangement of testing containers.

Figure 1 Experimental setup for slurry ice formation studies: (a) Freezing chamber with thermocouple placements; (b) Arrangement of right circular cylindrical containers for temperature and ice growth observation.

3.2 Dimensional Analysis

During freezing, the amount of ice forming, M_{Ice}, depends on several parameters which are the total mass of solution, $M_{Mixture}$, the container radius, R, the freezing point of the solution, T_{Freeze}, the freezing chamber temperature, $T_{Chamber}$, the operating time, t, the latent heat of fusion for ice, L, the specific heat of ice, Cp, and the properties of the mixture in liquid phase covering its thermal conductivity, $k_{Mixture}$, density, $\rho_{Mixture}$, and specific heat capacity, $Cp_{Mixture}$. The amount of ice formed is influenced by geometric, thermal, and time-dependent parameters. Then, mathematically,

$$M_{Ice} = f\,(M_{Mixture},\ R,\ T_{Freeze},\ T_{Chamber},\ t,\ L,\ Cp,\ k_{Mixture},\ \rho_{Mixture},\ Cp_{Mixture}) \quad (1)$$

Equation (1) involves a large number of variables. Therefore, dimensional analysis was employed in this study to reduce the number of variables in the physical problem by grouping them into dimensionless parameters. This approach broadened the applicability of the resulting equations, making them relevant across a wide range of conditions rather than limited to specific cases. Furthermore, the relationships among these dimensionless groups helped identify the key factors governing system behavior. Instead of requiring detailed experimentation for each variable, dimensional analysis identified a few critical dimensionless parameters that must be controlled, thereby simplifying the experimental process and significantly saving time and resources.

Dimensional analysis using the Pi theorem (Jebasingh, & Arasu, 2020) was conducted.All parameter units were converted into the fundamental units of mass, length, temperature, and time. The parameters were then systematically rearranged to eliminate each fundamental unit one by one, resulting in a dimensionless relationship. The final dimensionless form is:

$$\frac{M_{Ice}}{M_{Mixture}\,.Ste}=g\left(\frac{\alpha_{Mixture}\,.t}{R^2}\right) \tag{2}$$

where Ste is the Stefan number, $Ste = Cp(T_{Freeze} - T_{Chamber})/L$ and $\alpha_{\mathrm{Mixture}}$ is thermal diffusivity, $\alpha_{Mixture} = k_{Mixture}/\ (\rho_{Mixture}\ Cp_{Mixture})$. The Stefan number is a dimensionless parameter widely used in heat transfer analysis, especially in phase change processes such as melting and solidification. A high Stefan number indicates that a significant amount of sensible heat is required to change the system temperature before phase change phenomena, such as melting or freezing, become dominant. $(\alpha_{Mixture}.t)/R^2$. It is the key dimensionless parameter used to analyze transient freezing during slurry ice formation. A Stefan number value indicates that ice crystals can form more rapidly throughout the liquid.

The solution density, $\rho_{Mixture}$, could be found from the study of Rawat, & Pratihar (2018) and is also provided in the Appendix. The solution specific heat capacity, $Cp_{Mixture}$ and thermal conductivity, $k_{Mixture}$, could be taken from the weighted average values of water and FPD as follows:

$$Cp_{Mixture} = \frac{M_{Water}\,Cp_{Water} + M_{FPD}\,Cp_{FPD}}{M_{Mixture}} \tag{3}$$

$$k_{Mixture} = \frac{M_{Water}\,k_{Water} + M_{FPD}\,k_{FPD}}{M_{Mixture}} \tag{4}$$

Uncertainty Analysis

From the accuracies of all the instruments, the uncertainty of each dimensionless term could be evaluated by (Anderson, 1994).

$$R = f\,(x_1,\ x_2, \ldots x_n) \tag{5}$$

$$\omega_R = \left[\left(\frac{\partial R}{\partial x_1}\cdot\omega_1\right)^2 + \left(\frac{\partial R}{\partial x_2}\cdot\omega_2\right)^2 + \ldots + \left(\frac{\partial R}{\partial x_n}\cdot\omega_n\right)^2\right]^{1/2} \tag{6}$$

Where R is the output, $x_1,\ x_2,\ldots x_n$ are the measured parameters, $\omega_1,\ \omega_2,\ldots,\ \omega_n$ are the measured parameter accuracies, ω_R is the output uncertainty of which the maximum value in the experiments is less than 3%.

4. Results and Discussion

4.1 Ice and Slurry Ice Formation

Figure 2 shows the temperature histories during charging of working fluids which were water, water with 8 wt% ethanol and water with 8 wt% propylene glycol in the containers. The freezing chamber temperature was set at -20ºC. The starting time was defined as the moment when all working fluids reached approximately20ºC. The temperature of each working medium decreased with time until it reached its freezing point. After that, the temperature remained relatively steady during ice formation in the container, whereas the temperature for slurry ice continued to decline due to higher concentration of ethanol or propylene glycol in the liquid phase. The freezing point for water was 0 °C, while those of the water–ethanol and water–propylene glycol solutions were −2.6 °C and −2.3 °C, respectively, as reported by Rawat, & Pratihar (2018).

Figure 3 illustrates the relationship between the mass fraction of ice or slurry ice with total mass of working medium, $M_{Ice}\,/\,M_{Mixture}$, referred to as the "Ice packing factor (IPF)" over elapsed time. A higher concentration of FPD led to greater dispersion of FPD molecules throughout the water, which inhibited the formation of crystalline ice and promoted the growth of finer ice crystals or slurry ice (Ickes, & Cadwallader, 2017). However, as the ice was forming, higher concentration of the FPD in the rest of liquid solution resulted, then the freezing point was lower thereafter inhibiting further ice growth. Based on the experiments shown in Figures 3a and 3b, the IPF percentage increased with the concentration of ethanol or propylene glycol, reaching its peak at 8 wt% FPD concentration. Beyond this point, the IPF percentage declined with further increase in FPD concentration. Figure 3c showed higher ice formation rates with the use of FPDs compared to pure water. It was also observed that the water–ethanol solution outperformed the water–propylene glycol solution (Rawat, & Pratihar, 2018).

In thermal energy storage systems using ice, the inclusion of FPDs facilitates a higher ice formation rate during the charging process compared to pure water. This indicates the potential for achieving higher energy intensity in the storage system. However, it is essential to carefully select appropriate FPDs and determine their optimal concentration.

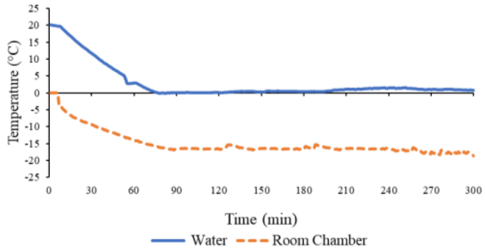

a. pure water

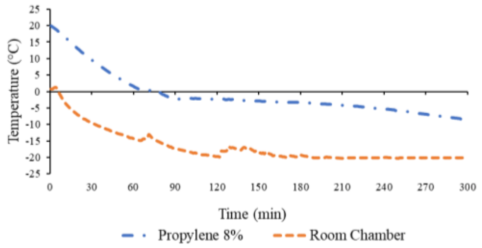

b. water with 8 wt% ethanol

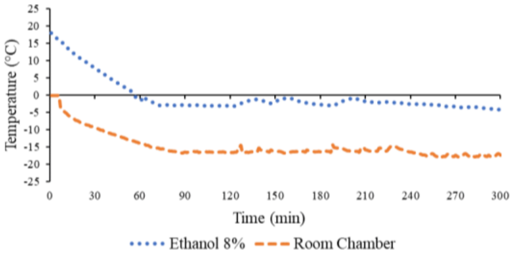

c. water with 8 wt% propylene glycol

Figure 2 Temperature evolution of working fluids during the freezing process at −20 °C: (a) Pure water, (b) Water with 8 wt% ethanol, and (c) Water with 8 wt% propylene glycol.

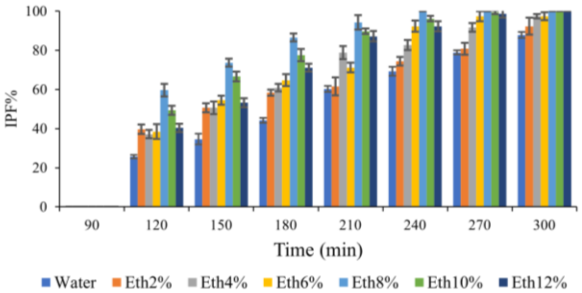

a. water-ethanol.

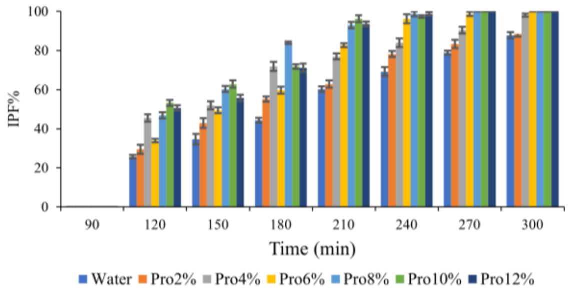

b. water-propylene glycol.

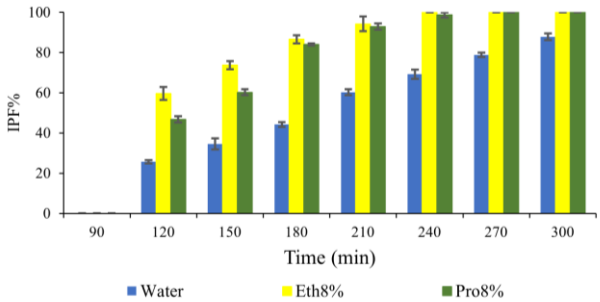

c. pure water, water with 8 wt% ethanol and water with 8 wt% propylene glycol.

Figure 3 Variation of Ice Packing Factor (IPF) over time: (a) Water–ethanol mixtures, (b) Water–propylene glycol mixtures, and (c) Comparison between pure water and 8 wt% FPD mixtures.

Figure 4 presents photographs of ice formation and the corresponding IPF percentages with time in case of pure water (Figure 4a) and slurry ice formation in case of water with 8 wt% ethanol (Figure 4b) and water with 8 wt% propylene glycol (Figure 4c). It could be seen that, for pure water, the ice crystal originated from the container surface and gradually spread towards the center. The crystal ice appeared clearer compared with the slurry ices during freezing from the aqueous solutions which had appeared opaque and dispersed and highly turbidity due to the FPD particles trapped in the solid ice as shown in Figure 5.

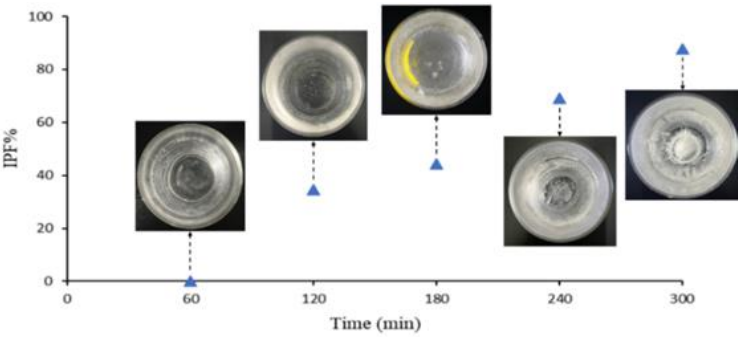

a. pure water

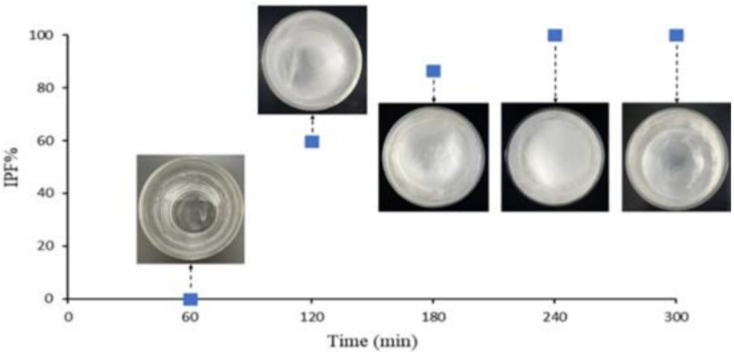

b. water with 8 wt% ethanol

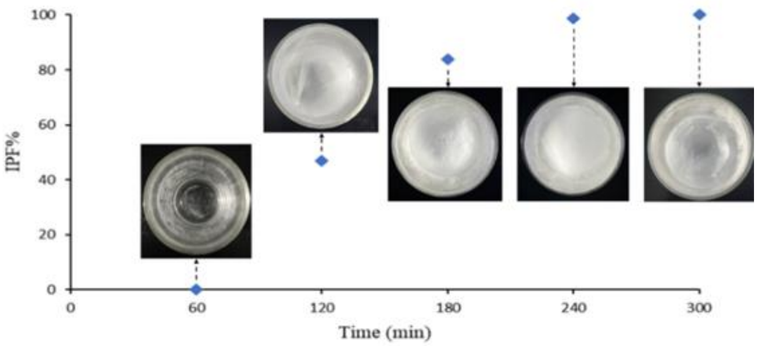

c. water with 8 wt% propylene glycol

Figure 4 Photographic evidence of ice and slurry ice formation correlated with %IPF over time: (a) Pure water, (b) Water with 8 wt% ethanol, and (c) Water with 8 wt% propylene glycol.

a. physical appearances of ice and slurry ice

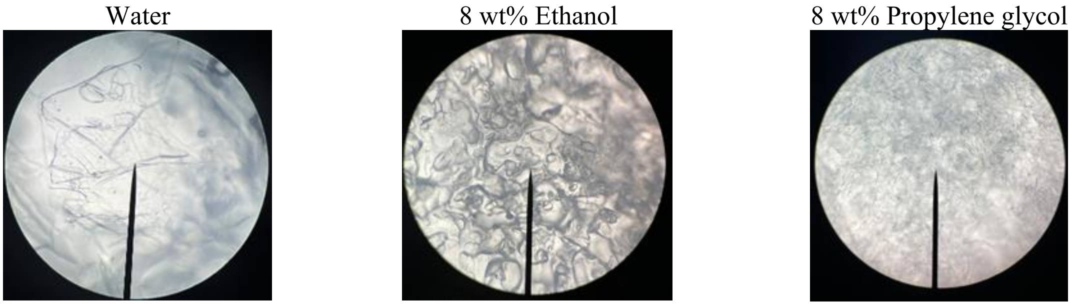

b. microscopic images of solid phases at 10× magnification.

Figure 5 Visual characteristics of ice and slurry ice: (a) Physical appearance of solid phases; (b) Microscopic images (10× magnification) of ice structures for pure water, ethanol- and propylene glycol-based mixtures.

4.2 Curve Fitting

Figure 6a shows the relationship between the dimensionless parameters during slurry ice formation for water ethanol and water–propylene glycol solutions with 0–12% FPD concentrations. The freezing chamber temperature was set between -15 to -20°C. It was straightforwardly found that the trend of M_{Ice} / ($M_{Mixture}$ .Ste) ratio increased with (α_{Mixture} .t) / R^2 for all conditions. Similar to Figure 3, increasing the FPD concentration from 0 to 8 wt% resulted in a higher M_{Ice} / ($M_{Mixture}$ .Ste) ratio, whereas further increases beyond 8 wt% led to a decline. In Figure 6a, the data plots were somewhat scattered. However, when the power of *Ste* was less, for example n = 0.5 and 0.9 for the FDP concentrations of 0 to 8 wt% and 8 to 12 wt%, respectively, as shown in Figure 6b, the data points were gathering into one line and the best fit was found with n = 0.01 and 0.71, respectively, of which the statistical coefficient of determination, R squared, was over 90% as shown in Figure 6c. The correlations among all parameters can therefore be expressed as:

For $0 \le x < 8$ wt%:

$$M_{Ice} = 0.3215 M_{Mixture} \left(Ste\right)^{0.01} \left(\frac{\alpha_{Mixture}\, t}{R^2}\right)^{1.0486} \tag{7}$$

For $8 \le x \le 12$ wt%:

$$M_{Ice} = 2.1165 M_{Mixture} \left(Ste\right)^{0.71} \left(\frac{\alpha_{Mixture}\, t}{R^2}\right)^{0.997} \tag{8}$$

where -20°C ≤ $T_{Chamber}$ ≤ -15°C.

The correlations presented in Equations (7) and (8) were used to predict the mass of slurry ice formed in right circular cylindrical containers with diameters of 5.6 cm and 6.6 cm, at various FPD concentrations in water–ethanol and water–propylene glycol solutions stored at −20 °C. The results, summarized in Table 1, indicated that at a given time interval, containers with larger diameters produced less slurry ice. This trend was attributed to the greater volume of working fluid in larger containers, which increased the time required for the temperature to reach the freezing point. Moreover, an FPD concentration of 8 wt% consistently resulted in the highest amount of slurry ice formation. The predicted results showed good agreement with the experimental data, with maximum deviations not exceeding 10%.

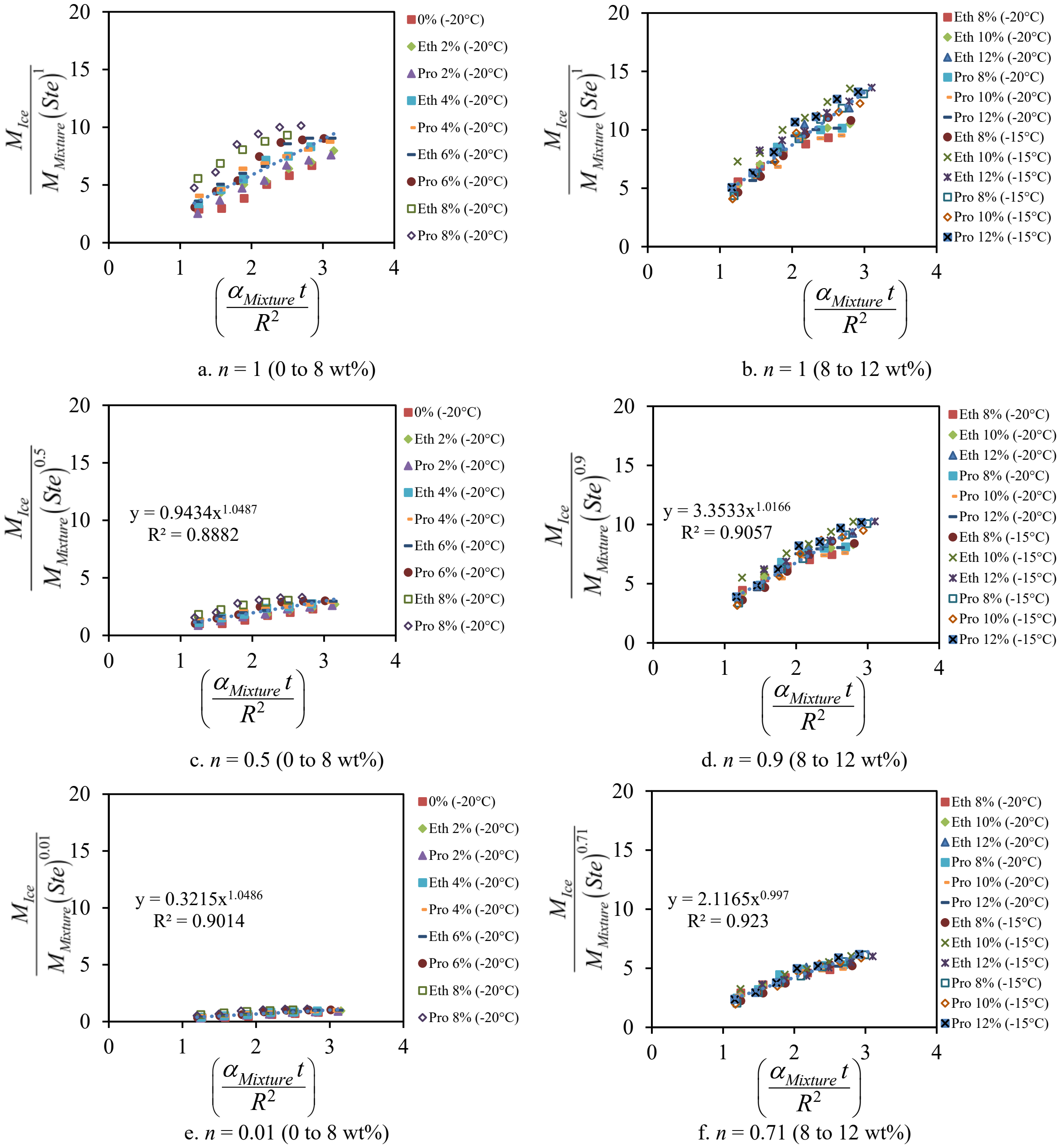

Figure 6 Empirical model fitting results showing dimensionless parameter relationships during ice formation: (a–f) Regression curves under varying Stefan number exponents for different FPD concentrations.

Table 1 Comparison of experimentally measured and empirically predicted slurry ice masses at various freezing point depressant (FPD) concentrations, operating times, and container diameters using water–ethanol and water–propylene glycol mixtures at −20 °C.

The diameter of beaker 5.6 cm								
% of mass	**Time (min)**	**Ethanol (Temperature -20 °C)**			**Propylene glycol (Temperature -20 °C)**			
		(Eq 7) **Cal (g)**	**Exp (g)**	**Error %**	(Eq 7) **Cal (g)**	**Exp (g)**	**Error %**
4%	210	111.72	120.00	-7.41	108.52	117.00	-7.82
	240	128.51	129.00	-0.38	124.83	131.00	-4.95
6%	210	111.79	111.00	0.70	107.39	117.00	-8.95
	240	128.59	140.00	-8.88	123.53	132.00	-6.86
		(Eq 8) **Cal (g)**	**Exp (g)**	**Error %**	(Eq 8) **Cal (g)**	**Exp (g)**	**Error %**
8%	210	138.42	147.00	-6.20	135.48	145.00	-7.03
	240	143.56	156.00	-8.67	154.77	154.00	0.50
10%	210	124.14	129.37	-4.22	134.84	148.00	-9.76
	240	141.81	150.00	-5.77	153.66	152.00	1.08
The diameter of beaker 6.6 cm							
		(Eq 7) **Cal (g)**	**Exp (g)**	**Error %**	(Eq 7) **Cal (g)**	**Exp (g)**	**Error %**
2%	210	106.05	105.00	0.99	103.70	103.00	0.67
	240	121.99	124.00	-1.65	119.28	118.89	0.33
6%	210	105.35	111.00	-5.37	101.20	100.00	1.19
	240	121.18	131.00	-8.10	116.41	126.00	-8.24
		(Eq 8) **Cal (g)**	**Exp (g)**	**Error %**	(Eq 8) **Cal (g)**	**Exp (g)**	**Error %**
8%	210	120.06	113.76	5.25	139.22	140.00	-0.56
	240	137.35	136.41	0.69	159.26	158.00	0.79
10%	210	107.30	104.19	2.90	129.02	133.00	-3.09
	240	125.91	127.87	-1.56	149.38	150.00	-0.42

5. Conclusion

Experiments were conducted to investigate slurry ice formation using water–ethanol and water–propylene glycol mixtures with various concentrations of freezing point depressant (FPD) in a right circular cylindrical container. The parameters influencing ice formation were correlated using the PI theorem, and the resulting developed models proved effective in predicting ice amount over time. The following findings are:

- Slurry ice exhibited a fluffy appearance with high turbidity in comparison to crystal ice, which appears clearer due to absence of trapped FPD particles.
- The quantity of ice formed increased with higher concentrations of ethanol or propylene glycol, peaking at an 8% FPD concentration. Subsequently, the ice growth declined with further increases in FPD concentration. Additionally, the ice formation rate was more favorable with water-ethanol solutions, compared with water-propylene glycol solutions.
- In ice thermal energy storage systems using FPDs, a faster ice formation rate was achieved during charging compared to pure water, potentially resulting in higher energy intensity. However, selecting appropriate FPDs and determining their optimal concentrations was essential.
- New empirical models, expressed in dimensionless form based on relevant parameters, were developed to predict slurry ice formation over time within a freezing chamber maintained at temperatures between −20 °C and −15 °C, and for FPD concentrations ranging from 0 to 12 wt%. To verify the accuracy of these models, additional experiments were conducted using solutions in containers of different sizes. The predicted results showed strong agreement with the experimental observations, confirming the reliability of the developed models.

6. Nomenclature

Cp_{FPD}	Specific heat capacity of depressant, J/kg·K
Cp_{Ice}	Specific heat capacity of ice, J/kg·K
$Cp_{Mixture}$	Specific heat capacity of mixture solution, J/kg·K
Cp_{Water}	Specific heat capacity of water, J/kg·K
k_{FPD}	Thermal conductivity of mixture solution, W/m·K
$k_{Mixture}$	Thermal conductivity of mixture solution, W/m·K
L	Latent heat of fusion, J/kg
M_{FPD}	Mass of depressant, kg
M_{Ice}	Mass of ice, kg
$M_{Mixture}$	Mass of mixture solution at initial condition, kg
R	Radius of container, m
Ste	Stefan number, dimensionless
$T_{Chamber}$	Temperature of freezing chamber, °C
T_{Freeze}	Freezing point of mixture solution, °C
t	Time, s
x	FPD concentration, wt%
$\alpha_{Mixture}$	Thermal diffusivity of mixture solution, m^2/s
$\rho_{Mixture}$	Density of mixture solution, kg/m^3

7. Acknowledgements

The authors wish to express their gratitude to the Graduate School for providing the TA/RA Scholarship, the Department of Mechanical Engineering, Faculty of Engineering, the Research Group for Renewable Energy, and the Fundamental Fund 2022 of Chiang Mai University for their valuable financial support of this research.

8. References

Afsharpanah, F., Ajarostaghi, S. S. M., & Arıcı, M. (2022a). Parametric study of phase change time reduction in a shell-and-tube ice storage system with anchor-type fin design. *International Communications in Heat and Mass Transfer*, *137*, Article 106281. https://doi.org/10.1016/j.icheatmasstransfer.2022.106281

Afsharpanah, F., Pakzad, K., Ajarostaghi, S. S. M., & Arıcı, M. (2022b). Assessment of the charging performance in a cold thermal energy storage container with two rows of serpentine tubes and extended surfaces. *Journal of Energy Storage*, *51*, Article 104464. https://doi.org/10.1016/j.est.2022.104464

Anderson, A. M. (1994). Experimental methods for engineers: JP Holman, McGraw-Hill, New York, NY, 1994, 616 pages, $44.75. *Experimental Thermal and Fluid Science*, *9*(2), Article 250. https://doi.org/10.1016/0894-1777(94)90118-X

Chavan, S., Rudrapati, R., & Manickam, S. (2022). A comprehensive review on current advances of thermal energy storage and its applications. *Alexandria Engineering Journal*, *61*(7), 5455-5463. https://doi.org/10.1016/j.aej.2021.11.003

Chen, M., Fu, D., Song, W., & Feng, Z. (2021). Performance of ice generation system using supercooled water with a directed evaporating method. *Energies*, *14*(21), Article 7021. https://doi.org/10.3390/en14217021

Fang, Y., Hua, L., Jin, C., Gao, J., & Han, Z. (2021). Analysis of the optimization on application of seawater slurry ice in coastal areas. In *3rd International Conference on Energy Resources and Sustainable Development (ICERSD 2020)*. EDP Sciences, Harbin, China. https://doi.org/10.1051/e3sconf/202123602023

Hamali, W., & Almusawa, M. Y. (2022). Transient heat transfer of NEPCM during solidification using Galerkin method. *Case Studies in Thermal Engineering*, *35*, Article 102114. https://doi.org/10.1016/j.csite.2022.102114

Hamzeh, H. A., & Miansari, M. (2020). Numerical study of tube arrangement and fin effects on improving the ice formation in ice-on-coil thermal storage systems. *International Communications in Heat and Mass Transfer*, *113*, Article 104520. https://doi.org/10.1016/j.icheatmasstransfer.2020.104520

Han, Z., Ma, Q., Fang, Y., Hua, L., Jin, C., & Huang, J. (2020). Progress and innovations of ice slurry generation based on scraped-surface method. *Journal of Physics: Conference Series*,1550(4), Article 042021. https://doi.org/10.1088/1742-6596/1550/4/042021

Hao, S., Zhou, W., Lu, J., & Wang, J. (2021). The optimal pumping power under different ice slurry concentrations using evolutionary strategy algorithms. *Energies*, *14*(20), Article 6738. https://doi.org/10.3390/en14206738

Ickes, C. M., & Cadwallader, K. R. (2017). Effects of ethanol on flavor perception in alcoholic beverages. *Chemosensory Perception*, *10*, 119-134. https://doi.org/10.1007/s12078-017-9238-2

Jebasingh, E. B., & Arasu, V. A. (2020). Characterisation and stability analysis of eutectic fatty acid as a low cost cold energy storage phase change material. *Journal of Energy Storage*, *31*. Article 101708. https://doi.org/10.1016/j.est.2020.101708

Kauffeld, M., Wang, M. J., Goldstein, V., & Kasza, K. E. (2010). Ice slurry applications. *International Journal of Refrigeration*, *33*(8), 1491-1505. https://doi.org/10.1016/j.ijrefrig.2010.07.018

Kumano, H., Asaoka, T., Saito, A., & Okawa, S. (2007). Study on latent heat of fusion of ice in aqueous solutions. *International Journal of Refrigeration*, *30*(2), 267-273. https://doi.org/10.1016/j.ijrefrig.2006.07.008

Kumano, H., Hirata, T., Shouji, R., & Shirakawa, M. (2010). Experimental study on heat transfer characteristics of ice slurry. *International Journal of Refrigeration*, *33*(8), 1540-1549. https://doi.org/10.1016/j.ijrefrig.2010.07.023

Li, Z., Leng, J., Talabany, Z. J., Abu-Hamdeh, N. H., Attar, E. T., Rothan, Y. A., ... & Hussin, A. M. (2023). Numerical modeling for phase change within storage system including adaptive grid. *Journal of Energy Storage*, *57*, Article 106227. https://doi.org/10.1016/j.est.2022.106227

Loem, S., Asanakham, A., Deethayat, T., Vorayos, N., & Kiatsiriroat, T. (2023). Testing of solar inverter air conditioner with PCM cool storage and sizing of photovoltaic modules. *Thermal Science and Engineering Progress*, *38*, Article 101671.

Mouneer, T. A., El-Morsi, M. S., Nosier, M. A., & Mahmoud, N. A. (2010). Heat transfer performance of a newly developed ice slurry generator: A comparative study. *Ain Shams Engineering Journal*, *1*(2), 147-157. https://doi.org/10.1016/j.asej.2011.05.004

Nguyen, X., & Tran, T. (2020). Experimental study on phase change materials for cold energy storage system. *Journal of Energy and Natural Resources, 9*(2), 51-55. https://doi.org/10.11648/j.jenr.20200902.11

Rahdar, M. H., Emamzadeh, A., & Ataei, A. (2016). A comparative study on PCM and ice thermal energy storage tank for air-conditioning systems in office buildings. *Applied Thermal Engineering*, *96*, 391-399. https://doi.org/10.1016/j.applthermaleng.2015.11.107

Rawat, K. S., & Pratihar, A. K. (2018). Thermo-physical properties of aqueous solution of ice slurry. *International Journal of Pure and Applied Mathematics*, *119*(17), 1493-1497.

Rayhan, F. A., Pamitran, A. S., Yanuar, & Patria, M. P. (2020a). Investigating the performance of ice slurry system and the growth of ice crystals using seawater. *Journal of Mechanical Science and Technology*, *34*, 2627-2636. https://doi.org/10.1007/s12206-020-0536-2

Rayhan, F. A., & Pamitran, A. S. (2020b). Effect of ice mass fraction on ice slurry flow for cold energy storage application. *Energy Reports*, *6*, 790-794. https://doi.org/10.1016/j.egyr.2019.11.159

Sandström, C. (2021). Frosting and defrosting on air source heat pump evaporators [Doctoral dissertation], Chalmers University of Technology.

San Khun, N., Deethayat, T., Kiatsiriroat, T., & Asanakham, A. (2025). Strategy for energy savings in a commercial building air-conditioning system with chilled water storage: A case study in a retail mall in Thailand. *Journal of Current Science and Technology*, *15*(1), 89-89. https://doi.org/10.59796/jcst.V15N1.2025.89

Sawicka, D., Cieśliński, J. T., & Smolen, S. (2020). A comparison of empirical correlations of viscosity and thermal conductivity of water-ethylene glycol-Al2O3 nanofluids. *Nanomaterials*, *10*(8), Article 1487. https://doi.org/10.3390/nano10081487

Thongwik, S., Vorayos, N., Kiatsiriroat, T., & Nuntaphan, A. (2008). Thermal analysis of slurry ice production system using direct contact heat transfer of carbon dioxide and water mixture. *International Communications in Heat and Mass Transfer*, *35*(6), 756-761. https://doi.org/10.1016/j.icheatmasstransfer.2008.02.007

Wang, M. J., & Kusumoto, N. (2001). Ice slurry based thermal storage in multifunctional buildings. *Heat and Mass Transfer*, *37*(6), 597-604. https://doi.org/10.1007/PL00005891

Yang, Y., Fu, S., Wu, W., & Zhang, B. (2020). Preparation and performance evaluation of a new type of binary shaped phase change material for buildings. *Chemical Industry and Engineering Progress*, *39*(10), 4119-4126.

Zhang, Y., Su, L., Dong, K., & Liu, T. (2019). Experimental study of ice slurry production system using direct contact heat transfer of RC318 and water in a horizontal pipe. *Energy Procedia*, *158*, 4495-4501. https://doi.org/10.1016/j.egypro.2019.01.762

Appendix A: Freezing points and densities of water-ethanol and water-propylene glycol mixture solutions (Mouneer et al., 2010)

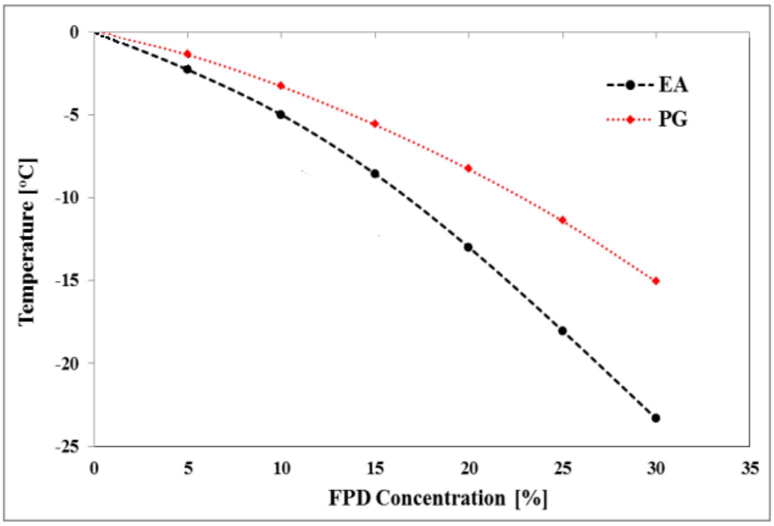

Figure A1 Freezing points of water-ethanol and water-propylene glycol (Mouneer et al., 2010)

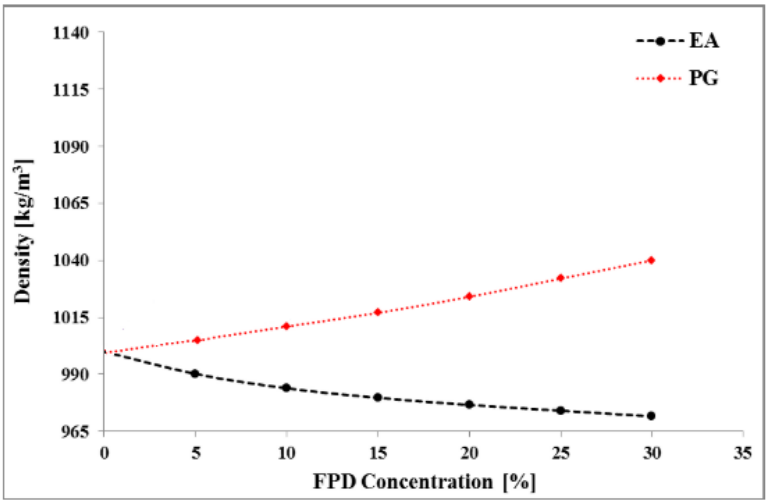

Figure A2 Density of water-ethanol and water-propylene glycol (Mouneer et al., 2010)